

Sensitivity Analysis of a Curved Heliostat Profile

Willem Landman

Dept. Mechanical and Mechatronic Engineering, Stellenbosch University

Solar Thermal Energy Research Group

Abstract

Curved heliostat facet optimization is one of twelve technology improvement opportunities mentioned in the Sandia Power Tower Technology Roadmap and Cost Reduction Plan and investigated here as to highlight the improvements possible to expand the state of the art. The analytical work done by Igel and Hughes regarding astigmatism of curved facets is revisited. An optical modelling tool has been developed in order to assess facet performance. The model is thorough and includes aspects which the analytical model neglects. The use of a Gaussian Function to characterize flux distribution of a facet image to allow comparisons is suggested. The influence of parameter variation on facet image size is presented and discussed. It is concluded that surface slope errors has an insignificant effect below a certain case specific threshold. The minimum image size of a non-dynamic facet is obtained by using a toroidal profile for both AZ and TA tracking cases. A centrally defocused toroidal facet profile is also investigated and is found to result in a more constant coefficient of optical aberration for a range of incidence angles. Although scope for alternative facet profile research exist, further investigations into accurate, practical and cost effective implementation of facet mounting is suggested as more important.

Keywords: Heliostat, Optics, Facet Profile, Aberration

1. Introduction

In a central receiver system, an array of heliostats focuses solar radiation onto a receiver aperture located at the top of a tower. The radiation is absorbed at the receiver and is transferred to a circulating fluid that reaches high temperatures and pressures. The fluid is transported either to a storage scheme or to a power conversion system to generate electricity. For large power generating cycles, it is advantageous to reach higher temperatures in order to increase power cycle efficiencies. A thermodynamic cycle called the SUNSPOT cycle has been developed that requires higher receiver temperatures ranging from 800 to 1100 °C.

In order to reach higher receiver temperatures, increased concentration ratios are required at the receiver [1]. Concentration ratio, equivalent to flux density at the receiver, is a summation of flux images of the individual heliostats. The flux density can be increased by either increasing the collector area or reducing the image sizes through improved optics of the heliostats in the field.

A flat heliostat facet creates a large image size equal to the normal projection increased by 9.3mrad sun-spread [2]. The image area can be reduced by using curved facets with a theoretical limit of 9.3mrad of sun-spread. Typically, spherical facet profiles are used. Spherically curved facet profiles suffer from astigmatism for nonzero incidence, which

increases with increased incidence angles [3]. This aberration is responsible for image distortion, increased image area and reduced flux densities [4]. Optimization of curved heliostat facets are thought to be able to reduce image sizes.

The Sandia Power Tower Technology Roadmap and Cost Reduction Plan highlights high temperature storage and more efficient high temperature power cycles as critical to driving costs down. Curved heliostat facet optimization is mentioned as one of twelve additional technology improvement opportunities regarding the solar collector field, which could help reduce the 8.6c/kWh projections to the 6c/kWh goal for the 2020 SunShot Initiative [5].

The sensitivity analysis aims to determine how the variability of different inputs will impact certain dependent variables. Apart from the surface profile, the optics' dependency on numerous factors ensures complexity. This paper primarily considers the sensitivity of these factors relative to the surface profile used. The analysis attempts to remain general to ensure that the outcomes are applicable to all cases. The validity of using circular profiles as the state of the art is assessed, and the possibility of improvement in optical quality through the use of alternative profiles is investigated.

The approach was to develop a ray tracing model which incorporates the following factors that influence the resultant facet image: facet profile, facet size, facet placement, surface slope errors, canting mechanism, tracking mechanism, tracking errors, structure stiffness, field position and sun position. A Gaussian Function is fitted to the flux density of the image and is described using six comparable parameters. A coefficient of optical aberration is also defined and used as a comparison measure.

2. Theoretical Heliostat Image Size Limits

This section, in part, revisits the comments made by Igel and Hughes in their frequently referenced paper [3]. For the purpose of simplicity, terminology used in this paper is sourced from Igel and Hughes[3].

2.1 Image of a Single Heliostat Facet

A flat heliostat facet creates a large image size equal to the normal projection increased by 9.3mrad sun-spread [2]. The image area can be reduced by using curved facets. A theoretical limit of 9.3mrad sun-spread exists. It is important to note that a practical heliostat does not need to project the sun image onto the collector and that defocusing is acceptable, however the more a facet image approximates that of the sun image, the smaller and more desirable the image. In order to quantify this, a Coefficient of Optical Aberration (COA) can be defined as the image size produced by a facet profile divided by the theoretical ideal. It is desired that the COA be minimized to the theoretical limit of 1.

Assuming a focal length of the slant range, the approximated image height and width limits of a spherical profiled facet is given by Igel and Hughes [3]:

$$h = w = 2D \sin^2 \left(\frac{\phi}{2} \right) + \beta_s d$$

The image sizes of a spherical facet profile divided by the theoretical limit results in COA's in both axes, $h/\beta_s d$ and $w/\beta_s d$, are given:

$$h/\beta_s d = w/\beta_s d = 2/(\beta_s F_r) \sin^2 \left(\frac{\phi}{2} \right) + 1$$

COA variation is plotted for a spherical facet profile in Figure 1. Here it can be seen that COA's are inversely proportional to focal ratio which defines the limits of a heliostat's size, and astigmatic aberration is dependent on the incidence angle ϕ .

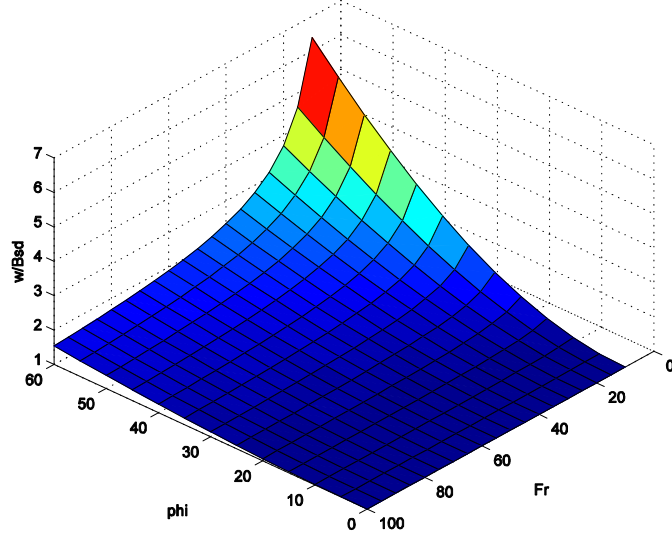


Fig. 1. COA of a spherical facet profile with focal length equal to the slant range.

In order to produce an ideal image at a nonzero incidence angle, a toroidal facet profile can be used, which has two different orthogonal radii of curvature. Igel and Hughes [3] define the ideal radii of curvature of an aligned toroidal facet in the sagittal and tangential planes as

$$r_s = 2d \cos \phi$$

$$r_t = 2d \sec \phi$$

Again the COA's, $h/\beta_s d$ and $w/\beta_s d$, can be plotted for an aligned toroidal facet using

$$\frac{h}{\beta_s d} = \frac{\cos \phi}{\beta_s F_r \cos \bar{\phi}} \left| \frac{\cos \bar{\phi}}{\cos \phi} - 1 \right| + 1$$

$$\frac{w}{\beta_s d} = \frac{\cos \phi}{\beta_s F_r} \left| 1 - \frac{\cos \phi}{\cos \bar{\phi}} \right| + 1$$

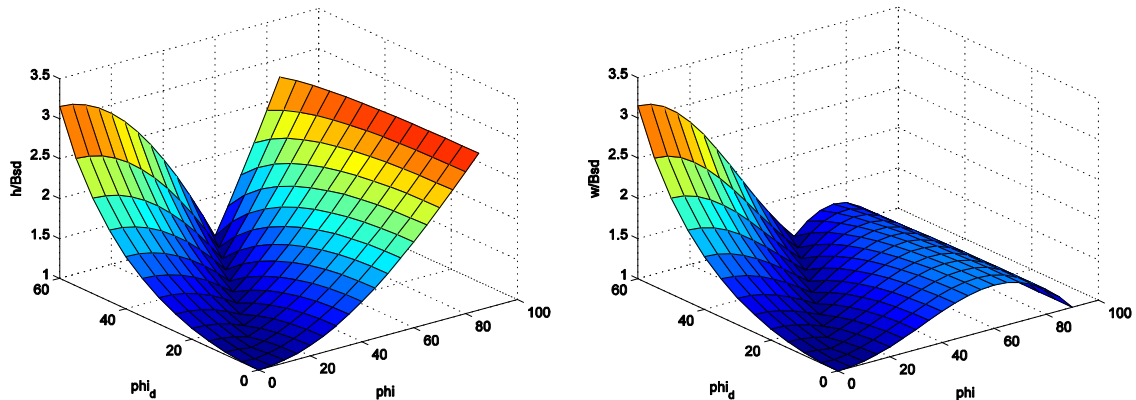


Fig. 2. COA for height and width of an aligned toroidal facet profile.

Two points need to be noted regarding the use of toroidal facet profiles. Firstly, the sagittal and tangential planes rotate around the heliostat normal if Azimuth Zenith tracking, which

is the industry standard, is used. Thus the given radii of curvature are not necessarily aligned to the tangential plane. Secondly, the radii of curvature are incident angle dependent, which also change throughout the day for both AZ and TA tracking. Since the incidence angle is both time of day and seasonally dependent, a toroidal facet profile will result in a perfect image only for a specific time of day or incidence angle $\bar{\phi}$, assuming the facet is aligned with the tangential plane. A toroidal facet whose radii of curvature are specified for the unique position and circumstances of the facet is thought to result in the minimum annual COA.

2.2 Image of a Multi-Faceted Heliostat

It is impractical to use very large facets on a heliostat. Larger heliostats are thus multi-faceted, where multiple facets are used to approximate the desired mirror profile. The alignment of the facets is referred to as canting. In addition to the image variation of the individual facet profiles, the canting of the facets also affects the image. The COA of a multi-spherically-faceted off axis canted [6] heliostat is given by [3]:

$$h/\beta_s d \cong \frac{\left(\frac{1}{\bar{F}_r} - \frac{1}{\bar{F}_r}\right)}{\beta_s} |1 - \cos\phi(\cos\bar{\phi}\sin^2\theta + \sec\bar{\phi}\cos^2\theta)| + 2/\bar{F}_r\beta_s \sin^2\left(\frac{\phi}{2}\right) + 1$$

$$w/\beta_s d \cong \frac{\left(\frac{1}{\bar{F}_r} - \frac{1}{\bar{F}_r}\right)}{\beta_s} |\cos\bar{\phi}\cos^2\theta + \sec\bar{\phi}\sin^2\theta| + 2/\bar{F}_r\beta_s \sin^2\left(\frac{\phi}{2}\right) + 1$$

The first term is defined by the canting mechanism and the second by the facet profile, indicating that facet profile and focal ratio of the facet still plays a role in COA for a multi-faceted profile. The outer facets have the largest effect on astigmatic aberration and are critical to the COA.

2.3 Surface Normal Optimization Study of a Facet Profile for Minimal Image Size

An independent optimization study was conducted in order to assess the validity of the claim that a toroidal facet will yield the theoretical minimal image size. 121 points arranged in an X-Y grid pattern on a square 5x5m heliostat facet were selected. A simplistic ray tracing model was written where the reflected rays from the specified points could be obtained while the surface normals of each point were treated as variable.

The annual sum of the perpendicular distance between the reflected ray from each point and the centre of the target was minimized through a genetic algorithm. The resulting optimized surface normals at given X and Y coordinates provided surface slope data that can be integrated to determine the original surface profile. The Frankot-Chellappa-algorithm was used to obtain Z values at the given points. A surface fitting tool could then be used to obtain the surface profile.

The analysis was conducted for both Azimuth-Zenith and Target Aligned tracking mechanisms. Both tracking mechanisms resulted in a toroidal facet profile with orthogonal radii of curvature. For AZ tracking case, the profile approximated a misaligned elliptical paraboloid, which was rotated by the toroidal mismatch angle θ around the z axis, while the TA tracking resulted in the same elliptical paraboloid but aligned with the mirror rack plane, as expected.

This result confirms that the minimum image size of a non-dynamic facet profile is obtained by using a toroidal facet profile for both AZ and TA tracking cases.

2.4 Alternate Facet Profiles

By minimizing the image size, flux densities are increased and spillage losses reduced leading to increased efficiencies. Increased flux densities have been regarded here as an optimum, however maximum flux must also be considered as a key design parameter [7]. The receiver design will be limited to a maximum flux density in order to protect the receiver from thermal stresses and material damages. Thus, though the image size is desired to be a minimum, flux distribution within the image may or may not be desired to be more uniform. A facet profile can be varied to achieve more uniform COA's as is discussed later.

It is suggested that the intercept factor is another important parameter of the optical efficiency of a heliostat, particularly for a Pressurized Volumetric Receiver with a Compound Parabolic Concentrator, where flux distribution is of lesser importance. The image variation can then be optimized for the specified receiver aperture and given heliostat position in the field, annually or for a specific season.

Scope does exist for the investigation of alternative profiles. Intuitively, an optimum surface profile must exist, however multiple optimums exist for variables that are dependent on the heliostat image variation. The optimization for flux uniformity and seasonal maximization of intercept factors where power requirements are influenced by seasonal demand variations are possible.

3. Modelling and Characterization of Facet Images

The analytical correlations presented previously define the image size limits using descriptive parameters for a simplified case. However other parameters, such as the flux distribution, cannot be extrapolated. Several parameters that were not considered have noticeable effects on the image. In order to quantify these parameters, the optics of a heliostat facet has been simulated. For the purpose of this paper, the analysis is limited to instantaneous imaging rather than time dependent and time averaged results.

The simulation uses a Monte Carlo type ray tracer written specifically for this application. It was desired that the ray data produced by the ray tracer be interpreted in such a way as to allow comparisons to other cases using specific "optical performance" parameters. Flux density was found from the ray data using a statistical binning strategy after which a Gaussian Function was fitted to the data. Six fitting parameters that best describe the flux density distribution were recorded as results. The stepwise progression resulting in the six parameter values are shown in Figure 3 and discussed in further detail below.

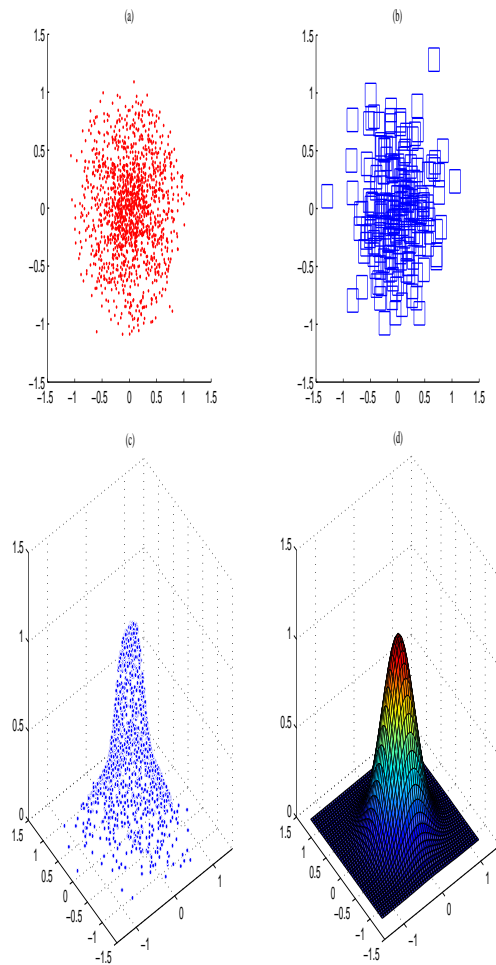


Fig. 3. (a) Ray intercept data, (b) Gaussian binning strategy, (c) Flux densities of the bins, (d) Gaussian surface fit.

3.1 Monte Carlo Ray Tracer

The purpose of the ray tracer is to represent only as accurately as is necessary the optics of the heliostat facet in order to be able to deduce the influence of individual variables on the parameter outputs. The ray tracing model is Monte Carlo based. A large number of rays are required to average out random number effects. Several iterations were conducted in order to find the number of rays for which the model results stabilize. This number was found to be in the order of magnitude $1e4$ rays. For purposes of the model, $3e4$ rays were used, given that the ray tracing model was computationally inexpensive.

The model accounts for both AZ and TA tracking mechanisms with tracking errors about the rotational and tilt axis, sun-shape variation, mirror slope and specular errors, facet shape, placement and profile as well as gravitational sag of torque tube and trusses. Atmospheric attenuation and absorbance losses have been omitted in the model. In order to eliminate cosine losses at the receiver, all simulations in this paper modelled the receiver as a flat disc with diameter D whose surface normal of axis of symmetry points toward the heliostat centre. The ray tracer was validated against SolTrace software.

3.2 Binning Strategy

In order to obtain the flux density at the data points, the target area is typically divided up into a grid based set of "Bins". The flux values of the rays that fall within each bin are

summed and divided by the bin area to obtain the flux density for that bin. Since the parameters needed to be generally comparable, it is required that the binning strategy be general and not image specific.

Though the common grid based binning strategy is easy to implement and fast, resolution problems could not be resolved when this strategy was used in an automated manner. It is suggested that user inputs are essential to ensure that resolution is maintained in areas of interest, specifically of high and low flux areas.

Instead, a statistical binning strategy was implemented as shown in Figure 3b. The number of bins were a given fraction of the number of ray intercept points. Bin positions were arranged according to normal distributions around the mean and variance of the ray intercept positions in both axes. Bin shapes were maintained as rectangular bins to be able to sort ray data, using two "if" statements rather than a sorting algorithm. The bin sizes were a function of the standard deviation in both axes. The bins sizes and number of bins were varied until sufficiently smooth results were obtained independent of number of rays or image size.

The significant advantage of the binning strategy used is that high resolution is obtained at the centroid of the image. Since the curve fitting algorithm deals with each data point with equal importance, fitting accuracy is higher around the image centroid where high flux densities occur.

3.3 Gaussian Fit

It is desired to be able to quantify the quality of a flux image produced by a heliostat. Related studies of facet canting methods [6, 8] generally consider the annual-incident-power-weighted-intercept (AIPWI). AIPWI is defined as the annual amount of solar radiation that intercepts the defined receiver aperture divided by the annual amount of radiation that arrives at the receiver and is thus solely a percentage measure of annual spillage losses. Jones considers AIPWI the best figure of merit to evaluate canting methods because of the direct tie to plant performance and economics [8]. However, to use AIPWI as a metric is inappropriate for a more detailed or generalized study since AIPWI is an annual performance outcome dependent on numerous free and case specific parameters.

The authors suggest a set of metrics that quantifies image quality from a given flux distribution. It is preferable that the image is able to be simplified and described using distinct parameters that have direct correlation to the image shape so that the parameters can have direct meaning and can be directly compared. The parameters should describe the deviation of the beam centroid from the aim point, the flux distribution characteristics of the image, and the image dimensions.

The curve fitting algorithm, used to find the desired parameters, uses an optimisation package to minimize the deviation of the given function to that of the flux density at a set of data points. The chosen approach uses the Trust-Region curve fitting algorithm to describe the flux density using a two dimensional Gaussian Function given below.

$$f(x, y) = Ae^{-(a(x-x_0)^2+2b(x-x_0)(y-y_0)+c(y-y_0)^2)}$$

where

$$a = \frac{\cos^2 \theta}{2\sigma_y^2} + \frac{\sin^2 \theta}{2\sigma_x^2} \quad b = \frac{\sin 2\theta}{2\sigma_y^2} + \frac{\cos 2\theta}{2\sigma_x^2} \quad c = \frac{\sin^2 \theta}{2\sigma_x^2} + \frac{\cos^2 \theta}{2\sigma_y^2}$$

The fitting algorithm results in values for the following parameters (see Figure 4):

- x_0 and y_0 , specify the location of the image centroid
- A is a flux density scaling factor
- θ accounts for the axis alignment
- σ_x and σ_y are the standard deviations of the flux density values along the new axes and indicate the ellipticity of the image

It must be noted that the function is not intended to accurately reproduce or mathematically represent the image but rather reduce the image to six parameters that can be compared in order to identify trends.

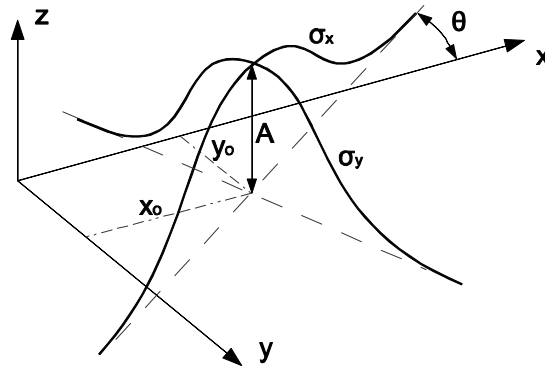


Fig. 4. Parameter influences on the Gaussian Function describing flux density.

3.4 Observed Data Anomalies

The use of the binning strategy results in a larger concentration of density points near the centroid of the image. During curve fitting, the centroid is thus weighted more heavily than the outer edges of the image. Figure 5 shows the observed anomaly for the overestimation of the standard deviation of very sharp images (left). This pronounced overestimation of the standard deviation occurs for low focal ratios below 5.

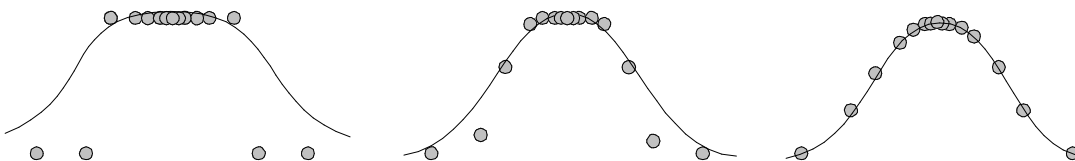


Fig. 5. Overestimation of standard deviation for sharp images at low focal ratios.

4. Results and Discussion

There are a large number of parameters of which their effects cannot all be shown here. COA is selected as the figure of merit given by the ratio of the resulting standard deviation to that of the ideal. The results presented here show only the variation of COA as a function of surface slope errors (SSE), structural deformation due to gravity (wilt) and incidence angle ϕ for various facet profiles.

Figure 6 depicts the case specific COA of a spherical facet profile as a function of SSE.

SSE are the angular deviations of the surface normals from the ideal. SSE are modelled as normal distributions and specified by their standard deviation in mrad. Initially at low SSE values, the COA is constant up to 0.7mrad, dominated by the astigmatic aberration effects of the spherical profile. This suggests that SSE below a certain case specific threshold are acceptable. After 0.7mrad, COA increases linearly with a gradient of 0.56 COA/mrad. SSE ranging between 0.3 and 4mrad are typical.

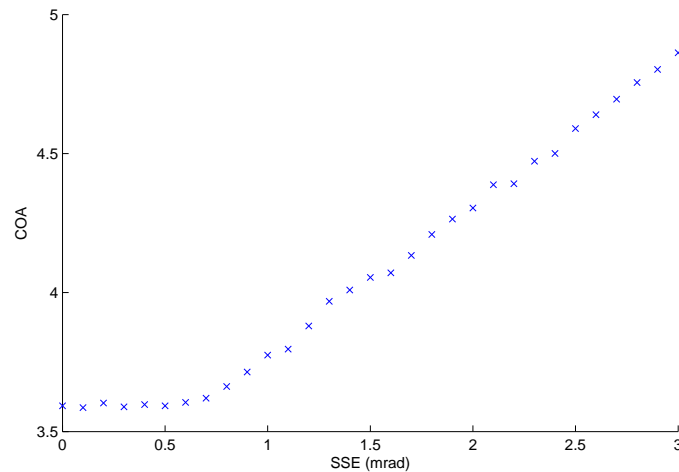


Fig. 6. Effect of Surface Slope Error variation on COA (Spherical Profile, $F_r = 40$, $\phi = 45^\circ$).

The deformation of the heliostat structure due to gravitational forces (wilt) was also considered in the model. Each heliostat has a unique structure, and in order to generalize the study, the deformation of both the trusses and tube were modelled as a uniformly distributed, simply supported, cantilevered beam. Only deformations normal to the surface were considered. Wilt is dependent on the orientation relative to the gravitational vector. The facet alignment, or canting, is done at a specific orientation which can be considered as the no load case, and variations from this case result in either positive or negative wilt.

For a more vertical orientation of the mirror rack plane, the gravitational force decreases below that of the alignment point, resulting in negative wilt. Inversely, at a more horizontal orientation, gravitational forces increase above that of the alignment point resulting in positive wilt. The gravitational loading will also be linked to the incidence angle, which is in turn directly dependent on the field position. Figure 7 shows a case for a heliostat that was facet aligned at $35^\circ \phi$ and currently oriented for a $30^\circ \phi$. Here the ratio of structure loading to stiffness varied. For a negative loading, indicating a more vertical orientation, a minimum is reached at the point where the structure decreases its radius of curvature to match that of the current ϕ . A positive loading has the effect of increased radii of curvature creating a further image aberration. Structural deformation is again case specific and can increase or decrease optical performance depending on the heliostat orientation for the range of incidence angles.

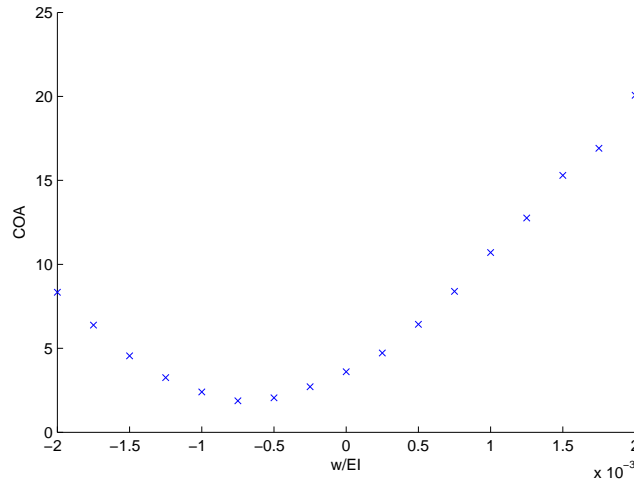


Fig. 7. Effect of Wilt on COA (Spherical Profile, $F_r = 40$).

The main influence on COA is the incidence angle ϕ . Figure 7 compares the COA variation to ϕ for 6 facet profiles. In practice, ϕ is never equal to zero since the heliostat will be in the shadow of the receiver and never 90. Rather, ϕ ranges between 0 and 90 depending on the heliostat position in the field and sun position. For a flat profile, the image is largest at a zero ϕ and decreases as ϕ increases due to the cosine effect. Inversely, the spherical and parabolic profiles produce a perfect image at a zero ϕ but are susceptible to astigmatic aberration for increased ϕ as predicted in Figure 1. The performances of the spherical and parabolic profiles approximate each other. This can be explained by the fact that a circle of radius R , with focal length $R/2$, given by

$$y = R - \sqrt{R^2 - x^2}$$

is easily approximated as a parabola of focal length $R/2$ through the Taylor expansion for values where $x \ll R$

$$y = \frac{x^2}{2R} - \frac{x^4}{8R^3} + \frac{x^6}{16R^5} - \dots \approx \frac{x^2}{2R}$$

The toroidal profile is tangentially aligned with the radius of curvature for alignment at 35° . COA is as expected lowest at ϕ of 35° and degrades in both directions as predicted in Figure 2. From Figure 8 it is clear that a toroidal facet profile of correct curvatures, which remain aligned (TA tracking), perform best for the required ϕ range.

Since the outer facets of the heliostat largely define the image size, focal length of facets closer to the heliostat centre can be varied or defocused within a certain range without affecting the overall image size. Such an adjustment would maintain the image size at increased ϕ but would increase image size at the alignment point. A toroidal facet profile centrally defocused gives a more constant COA over the ϕ range.

In order to obtain the theoretical ideal, a dynamic facet profile is required that changes shape depending on the sun position for the purpose of obtaining an aberration free image. As expected, the aberration free facet profile [9] maintains the ideal COA of 1.

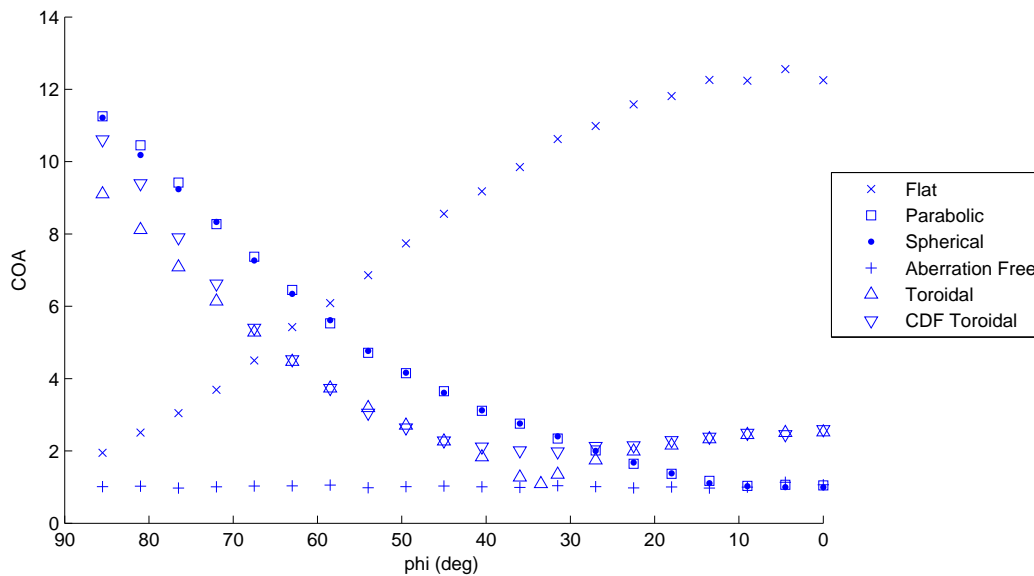


Fig. 8. COA of various facet profiles at varying incidence angles.

The correct and accurate implementation of the facet profiles is key to their function. Though improved performances can be modelled, practical implementation is not yet fully understood. Improving facet profiles does not necessarily increase cost since there are no additional components or material requirements, however manufacturing costs will increase as components become more specialized. If an inexpensive and accurate implementation method can be found to precisely mount custom facet profiles, significant improvements in COA and optical efficiency of the plant will result.

5. Conclusion

The theoretical limits of image sizes of both single and multiple faceted heliostats are reinvestigated. The minimization of the facet image size results in higher flux and reduced spillage losses.

A model was developed that can simulate the flux distribution of a heliostat facet image and describe it using six parameters. Apart from facet profile, other factors were also investigated: facet size, facet placement, surface slope errors, canting mechanism, tracking mechanism, tracking errors, structure stiffness, field position and sun position. Surface slope errors are found to be acceptable up to a case specific threshold. Structural deformation also affects optics and can result in increased or decreased optical performance dependent on heliostat orientation for the range of incidence angles.

Flat facet profiles result in high COA's. Spherical and parabolic profiles result in image degradation and increased COA for increased incidence angles. A surface normal optimization study showed that the minimum image size of a non-dynamic facet profile is obtained by using a toroidal facet profile for both AZ and TA tracking cases. The principal axis will be mirror rack aligned when TA tracking is used and misaligned by the toroidal mismatch angle when AZ tracking is used. A centrally defocused toroidal facet profile is also investigated and is found to result in a more constant COA for a range of incidence angles.

Facet profiles are shown to have significant effects on the image. Scope does exist for

investigations into alternative profiles for the variation of flux distribution in the focal spot. However, further research into accurately, practically and cost effectively implementing the facet profiles would be most beneficial. The effect of cost to performance benefit must be further studied before facet curvature improvements are further pursued. This research remains on-going.

Acknowledgements

We acknowledge with thanks the support for this work by the Solar Thermal Energy Research Group that made funds available through the solar spoke of the Department of Science and Technology, the National Research Fund and the Stellenbosch University Hope Project.

References

- [1] A. Rabl. Comparison of solar concentrators. *Journal of Solar Energy*, 18:93–111, 1976.
- [2] J. E. Parrott. Theoretical upper limit to the conversion efficiency of solar energy. *Solar Energy*, 21:227–229, 1978.
- [3] E. A. Igel and R. L. Hughes. Optical analysis of solar facility heliostat. *Solar Energy*, 22:283–295, 1979.
- [4] R. Zaibel, E. Dagan, J. Karni, and H. Ries. An astigmatic corrected target-aligned heliostat for high concentration. *Solar Energy Materials and Solar Cells*, 37:191–202, 1995.
- [5] G. J. Kolb, C. K. Ho, T. R. Mancini, and J. A. Gary. Power tower technology roadmap and cost reduction plan. Technical Report Albuquerque, Sandia Laboratories, 2011.
- [6] R. Buck and E. Teufel. Comparison and optimization of heliostat canting methods. *Journal of Solar Energy*, 131, 2009.
- [7] B.L. Kistler. A user's manual for delsol3: a computer code for calculating the optical performance and optimal system design for solar thermal central receiver plants. Technical report, SANDIA Labs: SAND86-8018, Albuquerque, 1986.
- [8] S. A. Jones. A comparison of on-axis and off-axis heliostat alignment strategies. Technical report, Sandia National Laboratories, 1996.
- [9] W. A. Landman and P. Gauché. Method for determining a continuous aberration free heliostat surface. In *South African Solar Energy Conference*, 2012.